HHS Public Access

Author manuscript

Nature. Author manuscript; available in PMC 2010 October 08.

Published in final edited form as:

Nature. 2010 April 8; 464(7290): 864–869. doi:10.1038/nature08849.

Molecular Mechanism of Multivesicular Body Biogenesis by ESCRT Complexes

Thomas Wollert and **James H. Hurley**

Laboratory of Molecular Biology, National Institute of Diabetes and Digestive and Kidney Diseases, National Institutes of Health, U. S. Department of Health and Human Services, Bethesda, MD 20892

Abstract

When internalized receptors and other cargo are destined for lysosomal degradation, they are ubiquitinated and sorted by the ESCRT complexes 0, I, II, and III into multivesicular bodies. Multivesicular bodies are formed when cargo-rich patches of the limiting membrane of endosomes bud inward by an unknown mechanism and are then cleaved to yield cargo-bearing intralumenal vesicles. The biogenesis of multivesicular bodies was reconstituted and visualized using giant unilamellar vesicles, fluorescent ESCRT-0, I, II, and III complexes, and a membrane-tethered fluorescent ubiquitin fusion as a model cargo. ESCRT-0 forms domains of clustered cargo but does not deform membranes. ESCRT-I and II in combination deform the membrane into buds, in which cargo is confined. ESCRT-I and II localize to the bud necks, and recruit ESCRT-0-ubiquitin domains to the buds. ESCRT-III subunits localize to the bud neck and efficiently cleave the buds to form intralumenal vesicles. Intralumenal vesicles produced in this reaction contain the model cargo but are devoid of ESCRTs. The observations explain how the ESCRTs direct membrane budding and scission from the cytoplasmic side of the bud without being consumed in the reaction.

It was shown thirty years ago that following stimulation, internalized EGF receptor localized to multivesicular bodies (MVBs) of human cells within minutes 1. Multivesicular bodies subsequently fuse with lysosomes where their contents are degraded 2, 3. Downregulation of cell surface receptors and transporters in yeast occurs by the same pathway, and yeast genetics identified the machinery responsible, now known as the ESCRT complexes 4–7. The ESCRTs also function in membrane remodeling reactions in the budding of HIV-1 and other enveloped viruses from the plasma membrane 8–10, and in the cleavage of the membrane neck between dividing cells from humans 11, 12 to a subset of Archaea 13. The ESCRT-III complex is required for MVB biogenesis, viral budding, and cytokinesis, and is responsible for the membrane cleavage step in the detachment of membrane buds into the lumen of the MVB 14. Ubiquitination is the principal signal for cargo to be directed into the

---

Correspondence and requests for materials should be addressed to J.H.H. (hurley@helix.nih.gov).

Author contributions T. W. carried out all experiments; T. W. and J. H. H. designed experiments and analyzed data; and J. H. H. wrote the manuscript.

MVB pathway. The upstream complexes ESCRT-0, I, and II contain ubiquitin (Ub)-binding domains (UBDs) which are responsible for interactions with ubiquitinated cargo 15, 16.

ESCRT-III proteins are capable of forming tubular structures 17–19, membrane evaginations 20, and budded intralumenal vesicles (ILVs) 14 in vitro or when overexpressed in cells. Most current thinking about the origin of membrane buds in MVBs has centered on the role of the ESCRT-III proteins 21. The attraction of these models is that ESCRT-III-induced buds have been directly observed in overexpression systems and in vitro. A major drawback to these models is that there is no satisfactory explanation of how ESCRT-III proteins can be rescued and recycled from self-induced buds. ESCRT-mediated membrane budding has been difficult to analyze in cells because deletion or knockdown of any of the essential ESCRT genes, whether upstream or downstream, leads to the formation of the aberrant class E compartment 7, 22. By electron microscopy, the class E compartment induced by deletion of subunits of ESCRT-0, -I, -II, and –III consists of stacked cisternae that are devoid of intralumenal vesicles 23–25 (G. Odorizzi, personal communication). These difficulties in resolving the mechanism of MVB biogenesis in vivo motivated us and others to reconstitute the pathway for analysis in vitro 14, 26, 27. Using reconstitution in giant unilamellar vesicles (GUVs), we now show that ESCRT-I and II together induce buds by stabilizing the bud neck. They recruit the ESCRT-III subunits Vps20 and Snf7 to the neck, but not the lumen of the bud, such that the bud can be cleaved from the exterior end of the neck with no loss of ESCRT complexes to the interior. Further, we find that ESCRT-0 forms large clusters of Ub on the membrane surface that are recruited to the bud necks by the ESCRT-I-II supercomplex. These observations provide the basis for a molecular mechanism of MVB biogenesis and cargo sorting that is fully consistent with biological observations.

Cargo clustering by ESCRT-0

Because the upstream ESCRT complexes contain UBDs, we wished to investigate whether they clustered ubiquitinated cargo, by analogy to other coat and adaptor systems in trafficking. In order to create a model system for endosomal cargo sorting, the C-terminus of Ub was fused to green fluorescent protein (GFP) or cyan fluorescent protein (CFP), and was tethered through an N-terminal polyhistidine tag to GUVs incorporating the Ni^{2+}-chelating lipid DOGS-NTA (Fig. 1a). Labeled yeast ESCRT-0 was found to co-localize with Ub in patches of up to 5 μm across (Fig. 1a). The increase in fluorescence of the rhodamine-PE membrane marker is due to clustering of the acidic dye with the basic tag on the cargo, as this effect is not seen when the uncharged membrane reporter BODIPY-PC is used (Supplementary Fig. 1). The ability of ESCRT-0 to cluster Ub is consistent with its pentavalent Ub binding through three UIMs and two VHS domains 28–32 (Ren & Hurley, submitted). Ub clustering is abrogated by the Ub mutation I44D (Fig. 1b), which disrupts the interaction with the UBDs of ESCRT-0 33, 34. This shows that Ub clustering is mediated by the direct interaction between Ub and the UBDs of ESCRT-0.

ESCRT-0 clustered on the membrane in domains whose size and number were enhanced by, but not completely dependent on, binding to Ub (Fig. 1c). This indicates that ESCRT-0 has an intrinsic ability to cluster on membranes. On the other hand, the clustering of Ub itself

depends absolutely on the integrity of the Ub Ile44 patch (Fig. 1d), consistent with the direct role of the ESCRT-0 UBDs. ESCRT-0 subunit Hrs contains a clathrin-binding motif 35 and localizes to extended, flat clathrin coats on endosomes 36. Our observations suggest that lateral self-organization is an intrinsic property of ESCRT-0, although it might be augmented or stabilized in the presence of clathrin. In contrast, isolated yeast ESCRT-I or II, which have two and one known UBDs, respectively 4, 15, 16, 37, 38, do not cluster Ub by themselves (Supplementary Fig. 2a, b), although as described below, the combination of the two together sometimes manifested small punctate Ub clusters. We infer from these data that ESCRT-0 is the main driving force for cargo clustering in the pathway.

ESCRT-I and II induce membrane bud formation and confine cargo

A central motivation for this study was to discover how the limiting membrane buds into MVBs. Addition of 15 nM each of ESCRT-I and –II together evaginated the membrane into numerous cargo-containing buds (Fig. 2a, b), although no single ESCRT complex by itself generated buds (Fig. 1a, 2c, Supplementary Fig. 2). The lumens of the GUVs were devoid of ILVs. The presence or absence of the upstream ESCRT-0 complex or the downstream ESCRT-III protein Vps20 did not markedly alter the number or character of buds formed (Fig. 2c, Supplementary Fig. 3), indicating that budding is a distinct activity of the ESCRT-I and –II pair. The presence of cargo was not required for ESCRT-I and II mediated budding (Supplementary Fig. 4). In contrast to ESCRT-I and II, which induce buds even at concentrations below their estimated levels in yeast cells (Supplementary Table 1), physiological concentrations of ESCRT-III subunits do not produce buds (Fig. 2c, Supplementary Fig. 5). We attribute our previous observation of ESCRT-III-induced buds 14 to the presence of up to 40-fold higher concentrations of subunits than used in this study.

The affinities of isolated ESCRT UBDs for Ub are in the range of Kd = 200 μM or lower, yet physiological ESCRT substrates are thought to typically be present in nM concentrations. Using 65 nM Ub-GFP, we assessed the ability of the upstream yeast ESCRTs to reduce the mobility of membrane-tethered Ub by FRAP microscopy. Ub-GFP in the limiting membrane quickly recovered following photobleaching (Supplementary Fig. 6). Exchange with Ub-GFP in bulk solution occurs under these experimental conditions, as a GUV photobleached in its entirety still was able to recover. About half of the cargo within ESCRT-0 Ub domains underwent exchange (Fig. 2d, e). The presence of ESCRT-I and II slowed the exchange of the mobile fraction by a factor of three, but did not alter the proportion of cargo capable of exchange. Cargo within the buds did not recover detectable fluorescence on the time scale of the experiment, regardless of the presence of ESCRT-0 (Fig. 2d, e, Supplementary Fig. 6). Therefore cargo is confined within the buds. The bud necks are still open to exchange with bulk solution (Supplementary Fig. 7, rows 2–4), so closure of the neck is not responsible for cargo confinement. These results indicate the cargo in the buds does not efficiently exchange through either lateral diffusion in the membrane or through the soluble phase.

ESCRT-I and II localize to the necks of membrane buds

ESCRT-I and ESCRT-II were diffusely localized in the absence of other ESCRTs (Fig. 2a, b), with ESCRT-I sporadically visible in concentrations at bud necks (data not shown). Addition of Vps20, the ESCRT-II binding subunit of ESCRT-III, strongly enhanced the localization of ESCRT-I and II at membrane buds without noticeably affecting the number or size of the buds. In the presence of Vps20, ESCRT-I (Fig. 3a) and ESCRT-II (Fig. 3b) were clearly visualized at membrane necks. No concentrations of ESCRT-I or II could be seen within the evaginated membrane buds. Tethered Ub was present within the evaginations and clustered in bright punctate structures at the neck connecting the evagination to the limiting membrane. The puncta of ESCRT-I and II co-localized with the bright puncta of Ub. The main conclusion derived from this experiment is that physiological low nM amounts of ESCRT-I and II produce extensive budding of membrane into the GUV lumen, without themselves entering the lumen. Rather, ESCRT-I and II localize to the neck of the bud, suggesting that they produce buds by inducing and stabilizing the bud necks.

Colocalization of Ub domains and membrane buds by ESCRT-0, -I, and -II

Having found that the upstream ESCRTs collectively carried out the key functions of Ub-cargo clustering and membrane budding, we sought to determine how these functions were coordinated. Labeled ESCRT-0 and Ub-CFP were monitored in the context of unlabelled ESCRT-I and II. ESCRT-I and II produced membrane buds, as seen also in the absence of ESCRT-0. The size and number of membrane buds did not change markedly from those generated in the absence of ESCRT-0 (Fig. 2c). Nor did the size and number of ESCRT-0-Ub domains markedly change upon addition of ESCRT-I and II (Fig. 1b). Most ESCRT-0-Ub domains were found co-localized with membrane buds (Fig. 4a). Co-localization of both buds with clusters and clusters with buds was sharply reduced in a mutant ESCRT-0 (ΔP(S/T)XP) 39, 40 that blocked the interaction between ESCRT-0 and –I (Fig. 4b, c). There were fewer ESCRT-0-Ub domains observed than membrane buds, probably because each ESCRT-0 domain involves more complexes than each membrane bud. Only 50 % of membrane buds were associated with ESCRT-0 domains (Fig. 4c), consistent with the greater number of buds. However, 80 % of the ESCRT-0 domains colocalized with at least one membrane bud (Fig. 4c). This observation confirms that the division of labor apparent for the isolated complexes or binary combinations, in which ESCRT-0 clusters cargo while ESCRT-I and II generate membrane buds, holds even when all three of the complexes are present simultaneously.

ESCRT-I-II bud necks recruit ESCRT-III subunits and activate scission

We previously reported that ESCRT-III subunits Vps20, Snf7, and Vps24, added in that order, had the intrinsic ability to scaffold their own bud neck and then cleave them 14. We sought to determine if the necks of buds scaffolded by ESCRT-I and II were competent to recruit ESCRT-III subunits, and if they supported ESCRT-III-mediated scission. The Vps20 subunit of ESCRT-III directly binds to and is activated by ESCRT-II on membranes 41, 42. In the presence of Vps20, little or no membrane scission is observed, consistent with the absence of ESCRT-III subunit Snf7, a critical scission factor (Fig. 5a). Under the same

conditions, except with unlabelled ESCRT-II, labeled Vps20 also localizes to bud necks. Labeled Vps20 is wholly absent from the membrane in the interior of the buds, and appears to be confined to the neck by its strong interaction with ESCRT-II. When labeled Snf7 is added to unlabelled ESCRT-0, -I, -II and Vps20, it is observed to colocalize with membrane necks and to be completely excluded from the interior membrane in the buds (Fig. 5b). Moreover, numerous ILVs are seen in the lumen of the GUV, indicating that scission of the membrane necks is occurring (Fig. 5c, Supplementary Fig. 7, row 5). This reaction occurs efficiently with only 15 nM of each component, while previous in vitro scission conditions lacking ESCRT-0 and –I required thirteen-fold more Snf7 in the presence of three-fold more ESCRT-II 42, or forty-fold more Snf7 in the absence of any upstream ESCRT complexes 14. ILVs generated in this reaction contain Ub-CFP, but are completely devoid of Snf7. The slowed reaction allowed us to visualize what we believe to be intermediates in the scission reaction, where Snf7 is localized to the bud necks and is poised for, or in the process of, severing the necks. When the third subunit important for scission, Vps24, was added, scission was efficient. Essentially all of the ILVs were detached from the limiting membrane (Supplementary Fig. 7, row 6), as expected.

Discussion

The observations in this study reveal a clear-cut division of labor between the ESCRT complexes. ESCRT-0 is primarily responsible for cargo clustering, the ESCRT-I-II supercomplex for membrane budding and cargo sequestration in buds, and ESCRT-III for scission.

The ESCRT-0 subunit Hrs is a component of flat coats with clathrin on endosomes prior to their maturation into MVBs 36. Such stiff, flat structures would seem to inhibit to formation of membrane buds. Having observed that ESCRT-I and –II membrane buds are associated with the edge of ESCRT-0-Ub domains in vitro, it now seems likely that in cells, buds form at the edge of an extended clathrin-ESCRT-0 coat 16. This suggests a model in which a large ESCRT-0-clathrin domain could serve as a cargo reservoir for buds spawned at the domain boundary. The driving force for cargo migration from the ESCRT-0 domain into the bud in the cellular setting remains to be discovered.

The biggest surprise and insight is that membrane buds are generated by ESCRT-I and –II, not ESCRT- III, contrary to widespread expectation. The membrane budding generated by high concentrations of ESCRT-III proteins is probably a byproduct of the physics of any curved filament with a membrane binding capacity 43. Rather, a supercomplex of ESCRT-I and II is responsible for membrane budding. The intimate cooperation of these two complexes, which act on the membrane as a single activity, is consistent with their high affinity for one another 44, co-assembly on membranes 45 and co-operativity in Ub-cargo interactions 37. ESCRT-I and –II are sufficient to sequester cargo in the buds, on the basis of FRAP analysis. It has been suggested that cargo is confined by a fence composed of ESCRT-III subunits 46. The present observations suggest that while ESCRT-III may abet cargo sequestration by stabilizing the ESCRT-I-II bud neck assembly and cleaving ILVs, ESCRT-I and –II are primarily responsible.

The lack of ESCRTs in the interior membrane of the buds shows that ESCRT –I and –II do not template buds by forming an interior coat. In other words, the ESCRTs do not act like "inside out" clathrin or COPII. The ILVs observed in this study are on the order of 2 μm in diameter, as compared to 25 nm for the largest molecular dimension of ESCRT-I, and mean diameters of 56 and 24 nm for human and yeast ILVs, respectively 25, 47. The disparity between in vitro and in vivo ILV sizes, and the absence of interior localized ESCRT-I and –II argues against the suggestion that ESCRT structures template ILV size 45. Other factors, notably tension and bending modulus, need to be considered. ESCRT-I and ESCRT-II (particularly as complexed with Vps20) contain multiple points of contact with membranes that are separated from each other by rigid stalks on the order of 15 nm 42, 45, 48, 49. These separations correspond to reasonable dimensions for a membrane neck.

In the reconstitution reported here, scission occurs with minimal or no internalization of ESCRTs. There have been no consistent reports of ESCRTs localized within MVBs, and all available evidence shows that to the contrary, ESCRTs are continuously recycled and used in multiple rounds of scission. When ILV budding and scission is driven in vitro by ESCRT-III alone, ESCRT-III was localized both within and outside ILVs, and the portion localized within was consumed in the reaction. In the presence of ESCRT-I and –II, ESCRT-III stays outside the bud, consistent with observations in cells. The unusual ability of ESCRT-III to cleave from outside the bud depends on its restricted localization to the neck. ESCRT-III has been visualized at midbodies connecting dividing cells 11, 12, and ESCRT-III has been modeled as an interior collar capable of severing the neck from within 50Similarly, it has been widely expected that ESCRT-III would form a collar lining the inside of the neck of nascent HIV-1 virions where they attach to the plasma membrane of T-lymphocytes and macrophages 9, 10, 19, and at the connection between the limiting membrane of the MVB and nascent ILVs 15, 21. In this regard, it is satisfying to directly visualize ESCRT-III localization to the neck of budding ILVs. These observations are consistent with the concept that ESCRT-III severs nascent HIV-1 virions from the plasma membrane, and cuts membranous connections between dividing cells, through the same type of neck-constricting activity.

In summary, ubiquitinated cargo sorting into MVBs by the ESCRTs has been reconstituted using purified components in a reaction that mirrors the known biological properties of the pathway and violates none of them. ESCRT-0 forms large domains of clustered cargo, consistent with its polyvalent Ub binding and its known participation in flat clathrin coats in early endosomes, upstream of the rest of the ESCRT pathway (Fig. 6a). ESCRT-I and –II, whose molecular function has been ill- defined, are responsible for membrane budding into the lumen of the MVB. ESCRT-I and II appear to act by an unusual mechanism in which their rigid multivalent membrane-binding structures may template the formation of bud necks (Fig. 6c). We envision the large ESCRT-0-cargo domain acting as a cargo reservoir for a succession of smaller ESCRT-I-II buds until the cargo is all internalized and the coat disassembles. ESCRT-III has a highly restricted localization to the membrane neck and carries out scission efficiently even at low nanomolar concentrations (Fig. 6d), confirming the concept of ESCRT-III as a scission machine for membrane necks.

METHODS SUMMARY

Protein purification and labeling

The recombinant ESCRT-0 complex was expressed in yeast and purified using Ni-NTA affinity chromatography and gel filtration (Supplementary Fig. 8). ESCRT-I, -II, Vps20, and Snf7 were expressed in bacteria and purified as previously described 14, 45, 49. ESCRT-0, -I, and –II were labeled with Alexa 488 on native Cys residues, and the engineered Vps20 N85C and Snf7 N-term Cys were labeled on introduced Cys residues.

In vitro MVB biogenesis reactions

GUVs were prepared essentially as described 14 with the addition of 5 % (mol/mol) Ni-NTA-DOGS and a corresponding reduction in the mole fraction of POPC. A 200 µl observation chamber (Lab-Tek chambered #1.0 Borosilicate) was coated using 5 mg/ml BSA to avoid distortion of GUVs upon contact with the bottom of the chamber and rinsed with buffer (50 mM Tris HCl pH 7.4, 300 mM NaCl). 100 µl of GUVs were incubated with 130 nM His_6-GFP-Ub (for FRAP experiments) or His_6-CFP-Ub (for all other experiments) for 15 min, mixed with 100 µl of the first ESCRT complex to be added (15 nM final concentration), and incubated for 5 min. The buffer and all proteins added to GUVs matched the osmolarity of the GUV solution (~650 mOsm due to evaporation of ~10% water during electroformation at 60°C). The other ESCRT-complexes or ESCRT-III subunits were added to the GUV-buffer mixture to yield a final concentration of 15 nM. The solution was stirred to accelerate protein distribution and binding. All steps of protein addition were separated by 5 min incubation intervals at room temperature. One buffer control was performed for each experiment. This control was treated exactly like that of the actual experiment, however, only buffer and no ESCRT proteins was added. Stirring and incubation was the same for control and experiment.

METHODS

Lipids and dyes

The following lipids were purchased from Avanti Polar Lipids: 1-palmitoyl-2-oleoyl-sn-glycero-3-phospho-L-serine (POPS), 1-palmitoyl-2-oleoyl-sn-glycero-3-phosphocholine (POPC), cholesterol, 1,2-dioleoyl-sn-glycero-3-[(N-(5-amino-1-carboxypentyl)iminodiacetic acid)succinyl] (nickel salt; Ni-NTA DOGS), 1,2-dipalmitoyl-sn-glycero-3-phosphoethanolamine-N-(lissamine rhodamine B sulfonyl). Phosphatidylinositol 3-phosphate diC16 (PI(3)P) was purchased from Echelon. Thiol-reactive Alexa (Alexa Fluor 488 C5 maleimide) and BODIPY-FL-C5-HPC were from Molecular Probes.

Cloning, expression and purification of proteins

DNA encoding ESCRT-0 subunits Hse1 and Vps27 was amplified by PCR from *Saccharomyces cerevisiae* genomic DNA and cloned into the pESC-Ura yeast expression vector (Stratagene). Hse1 was expressed fused to an N-terminal His_6-tag followed by a TEV protease cleavage site. The construct was transformed into the protease deficient yeast strain DDY1810 (a gift from Beverly Wendland, Johns Hopkins University, Baltimore). The yeast culture was grown to an OD at 600 nm of 0.8 in YNB supplemented with 2% (w/w)

raffinose, 20 mg/l tryptophan, and 30 mg/l leucine at 30°C. Expression of ESCRT-0 was induced by addition of 2% (w/w) galactose, 20 g/l yeast extract, and 15 g/l bacto tryptone. The complex was expressed at 28°C for 16 hours and purified using Ni-NTA resin (Qiagen) and eluted with 100 mM imidazole. Elution fractions were cleaved using TEV-protease and further purified by gel filtration (Superdex 200 column) and a second affinity step (Ni-NTA resin). Pooled fractions of ESCRT-0 were concentrated to 7 μM, flash frozen in liquid nitrogen and stored at −80°C until use. The three PSDP-like motifs in Vps27 were mutated to AAAA (positions 427–430, 504–507, and 561–564) using the QuickChange Multi site directed mutagenesis kit (Stratagene) and the mutant ESCRT-0 complex was purified as described for the wild-type protein. The His_6-Ub-GFP and CFP fusion proteins used in this study were the kind gift of Evzen Boura (NIDDK, NIH).

Full length yeast ESCRT-I and -II, subcloned into the pST39 vector, were transformed into Rosetta pLys cells and grown in LB-medium at 37°C until an optical density at 600 nm of 0.8 was reached. Expression was induced by addition of 0.5 mM IPTG at 18°C and the cultures were grown for an additional 16 hours. The complexes were purified by Ni-NTA affinity chromatography (His6-tag fused to Vps23 of ESCRT-I and Vps22 of ESCRT-II) and the tags were removed by digesting elution fractions with Tev protease. The complexes were further purified using size exclusion chromatography (Superdex 200 16/60 columns, GE Healthcare), with 50 mM Tris pH 7.4 and 300 mM NaCl as running buffer. Aliquots of all purified proteins were immediately flash frozen in liquid nitrogen and stored at −80°C. ESCRT-III subunits Vps20 and Snf7 were cloned into the pHis2 vector, containing MBP in between the His-tag and the TEV cleavage site. Cultures were grown at 37°C until an optical density at 600 nm of 0.8, induced with 0.5 mM IPTG and incubated at 30°C for 3 hours. The MBP-fusion proteins were purified using Ni-NTA affinity chromatography and elution fractions were cleaved with TEV protease for 2 hours at room temperature. The digested fractions were subjected to size exclusion chromatography and further purified using a second affinity purification to remove traces of uncleaved protein and TEV protease. Snf7 was maintained at concentrations ~8μM and immediately flash frozen in liquid nitrogen. Vps20 was concentrated to 20μM, frozen in liquid nitrogen and stored at −80°C until use. The His6-Ub-GFP and CFP fusion proteins used in this study were the kind gift of Evzen Boura (NIDDK, NIH). The I44D mutation was introduced using the QuickChange site directed mutagenesis kit (Stratagene) and the mutant was expressed and purified as described for the ESCRT-I and -II complexes.

Fluorescent labeling of proteins

To label Vps20 and Snf7 a cysteine residue was introduced by mutating Asn85 (Vps20) or inserted at the N-terminus immediately after the start codon (Snf7) using the QuickChange Mutagenesis Kit (Stratagene) according to the manufacturer's protocol. ESCRT-0, -I, and –II were labeled using their native Cys residues. The purified and concentrated proteins were labeled by incubating Alexa Fluor 488 C5 maleimide at a molar ratio of 1:1 with the protein at 30°C for one hour under a N_2 atomosphere. The labeled fraction was determined by running samples on an SDS-PA gel and fluorescence scans of the gel in a Typhoon variable mode imager (GE-Healthcare) using 488 nm excitation and 495 nm detection wavelengths. Quantification of labeling efficiency was achieved by separating excess of dye from labeled

protein using two consecutive HiTrap Desalting Columns (GE-Healthcare). Molar protein and Alexa488 concentrations of the purified protein were determined using absorption at 280 and 495 nm, respectively. Labeling efficiencies for all reactions exceeded 90 %.

Preperation of giant unilamellar vesicles (GUVs)

A thin film of lipid mixtures containing POPC (57 mol%), POPS (10 mol%), cholesterol (25 mol%), PI(3)P (3 mol%), Ni-NTA DOGS (5 mol%) and lissamine-rhodamine-PE (0.1 mol %) was applied to indium-tin oxide covered glass slides and placed into a self-made Teflon chamber. The glass slides were separated by a 2 mm thin glucose solution (600 mM) and an AC electric field (1V, 10 Hz) was applied for 4 h at 60°C following the previously described GUV electroformation protocol 51. The GUVs were harvested after cooling down to room temperature and used immediately.

In vitro MVB biogenesis reactions

GUVs were prepared essentially as described 14 with the addition of 5 % (mol/mol) Ni-NTA-DOGS and a corresponding reduction in the mole fraction of POPC. A 200 µl observation chamber (Lab-Tek chambered #1.0 Borosilicate) was coated using 5 mg/ml BSA to avoid distortion of GUVs upon contact with the bottom of the chamber and rinsed with buffer (50 mM Tris HCl pH 7.4, 300 mM NaCl). 100 µl of GUVs were incubated with 130 nM His_6-GFP-Ub (for FRAP experiments) or His_6-CFP-Ub (for all other experiments) for 15 min, mixed with 100 µl of the first ESCRT complex to be added (15 nM final concentration), and incubated for 5 min. The buffer and all proteins added to GUVs matched the osmolarity of the GUV solution (~650 mOsm due to evaporation of ~10% water during electroformation at 60°C). The other ESCRT-complexes or ESCRT-III subunits were added to the GUV-buffer mixture to yield a final concentration of 15 nM. The solution was stirred to accelerate protein distribution and binding. All steps of protein addition were separated by 5 min incubation intervals at room temperature. One buffer control was performed for each experiment. This control was treated exactly like that of the actual experiment, however, only buffer and no ESCRT proteins was added. Stirring and incubation was the same for control and experiment. Randomly chosen fields of view were evaluated to reveal the number of membrane buds and ILVs per GUV. Reactions were performed as described above and all GUVs in the particular fields of view were scanned in the z direction. All membrane buds or ILVs per GUV were counted, and for each experimental condition 80 to 100 GUVs were analyzed, except for results in Fig. 4c, which were based on 70 to 80 GUVs per experiment. Results were summarized in histograms. Histograms in figures show results from a single experiment. All experiments were repeated in triplicate yielding essentially identical numbers of buds and ILVs in each replicate.

Confocal fluorescence microscopy

Images were taken in multi-tracking mode on a Zeiss LSM510 or Confocor laser-scanning confocal microscope with a 63× Plan Apochromat 1.4 NA objective and a 488/543 or 458 dichroic mirror at a resolution of 512 × 512 pixel. The GFP/Alexa-488 dyes or CFP were excited using the 488 nm or 458 nm line and rhodamine was excited with a 543 nm HeNe laser. GFP/Alexa488 emission was collected with a 505–530 nm bandpass filter and CFP using a 470–500 nm bandpass filter. Rhodamine emission was collected with a 560 nm

longpass filter. The pinholes for each channel were set for an approximate 1.5 – 2.5 μm optical slice. Laser power was 9 μW for the 543 nm channel and 24 μW for the 458 and 488 nm channels. Images were analyzed using the LSM Examiner software.

Fluorescence recovery after photobleaching

GUVs were incubated with His_6-GFP-Ub and ESCRT complexes (as indicated in Fig. 2, S3) and as described above. Experiments were performed using a LSM510 laser scanning confocal microscope with a 63× Plan Apochromat 1.4 NA objective and a 488/543 dichroic mirror at a resolution of 124 × 124 pixel with three-fold zoom and an open pinhole. GFP was excited using the 488 nm laser line and 14 μW for imaging before and after bleaching. GFP fluorescence was bleached using 100 % laser power of the 458 nm, 488 nm, and 514 nm laser lines for 20 iterations. Recovery was observed by scanning at 488 nm every 149 msec for at least 50 sec. Fluorescence intensities were determined using the LSM Examiner software. For the analysis shown in Fig. 2, 10 FRAP curves of 10 buds or clusters, respectively, from 10 different GUVs were used.

Supplementary Material

Refer to Web version on PubMed Central for supplementary material.

Acknowledgements

We thank E. Boura for producing the CFP-Ub and GFP-Ub, J. Lippincott-Schwartz for microscope access, B. Wendland for a yeast strain and advice, and W. Prinz for comments on the manuscript. This work was funded by the Intramural Program of the National Institutes of Health, National Institute of Diabetes and Digestive and Kidney Diseases and Intramural AIDS Targeted Antiviral Program to J.H.H. and an EMBO long term fellowship to T.W.

References

1. Haigler HT, McKanna JA, Cohen S. Direct Visualization of the Binding and Internalization of a Ferritin Conjugate of Epidermal Growth-Factor in Human Carcinoma-Cells a-431. J. Cell Biol. 1979; 81:382–395. [PubMed: 313931]
2. Gruenberg J, Stenmark H. The biogenesis of multivesicular endosomes. Nat. Rev. Mol. Cell Biol. 2004; 5:317–323. [PubMed: 15071556]
3. Piper RC, Katzmann DJ. Biogenesis and function of multivesicular bodies. Annu. Rev. Cell Devel. Biol. 2007; 23:519–547. [PubMed: 17506697]
4. Katzmann DJ, Babst M, Emr SD. Ubiquitin-dependent sorting into the multivesicular body pathway requires the function of a conserved endosomal protein sorting complex, ESCRT-I. Cell. 2001; 106:145–155. [PubMed: 11511343]
5. Babst M, Katzmann DJ, Snyder WB, Wendland B, Emr SD. Endosome-associated complex, ESCRT-II, recruits transport machinery for protein sorting at the multivesicular body. Dev. Cell. 2002; 3:283–289. [PubMed: 12194858]
6. Babst M, Katzmann DJ, Estepa-Sabal EJ, Meerloo T, Emr SD. ESCRT-III: An endosome-associated heterooligomeric protein complex required for MVB sorting. Dev. Cell. 2002; 3:271–282. [PubMed: 12194857]
7. Bowers K, Stevens TH. Protein transport from the late Golgi to the vacuole in the yeast Saccharomyces cerevisiae. Biochim. Biophys. Acta Mol. Cell Res. 2005; 1744:438–454.
8. Morita E, Sundquist WI. Retrovirus budding. Annu. Rev. Cell Devel. Biol. 2004; 20:395–425. [PubMed: 15473846]

9. Fujii K, Hurley JH, Freed EO. Beyond Tsg101: the role of Alix in 'ESCRTing' HIV-1. Nat. Rev. Microbiol. 2007; 5:912–916. [PubMed: 17982468]
10. Bieniasz PD. The Cell Biology of HIV-1 Virion Genesis. Cell Host Microbe. 2009; 5:550–558. [PubMed: 19527882]
11. Carlton JG, Martin-Serrano J. Parallels between cytokinesis and retroviral budding: a role for the ESCRT machinery. Science. 2007; 316:1908–1912. [PubMed: 17556548]
12. Morita E, et al. Human ESCRT and ALIX proteins interact with proteins of the midbody and function in cytokinesis. EMBO J. 2007; 26:4215–4227. [PubMed: 17853893]
13. Samson RY, Bell SD. Ancient ESCRTs and the evolution of binary fission. Trends Microbiol. 2009; 17:507–513. [PubMed: 19783442]
14. Wollert T, Wunder C, Lippincott-Schwartz J, Hurley JH. Membrane scission by the ESCRT-III complex. Nature. 2009; 458:172–177. [PubMed: 19234443]
15. Hurley JH. ESCRT Complexes and the Biogenesis of Multivesicular Bodies. Curr. Opin. Cell Biol. 2008; 20:4–11. [PubMed: 18222686]
16. Raiborg C, Stenmark H. The ESCRT machinery in endosomal sorting of ubiquitylated membrane proteins. Nature. 2009; 458:445–452. [PubMed: 19325624]
17. Lata S, et al. Helical Structures of ESCRT-III are Disassembled by VPS4. Science. 2008; 321:1354–1357. [PubMed: 18687924]
18. Pires R, et al. A Crescent-Shaped ALIX Dimer Targets ESCRT-III CHMP4 Filaments. Structure. 2009; 17:843–856. [PubMed: 19523902]
19. Bajorek M, et al. Structural basis for ESCRT-III protein autoinhibition. Nat. Struct. Mol. Biol. 2009; 16 754-U95.
20. Hanson PI, Roth R, Lin Y, Heuser JE. Plasma membrane deformation by circular arrays of ESCRT-III protein filaments. J. Cell Biol. 2008; 180:389–402. [PubMed: 18209100]
21. Hanson PI, Shim S, Merrill SA. Cell biology of the ESCRT machinery. Curr. Opin. Cell Biol. 2009; 21:568–574. [PubMed: 19560911]
22. Raymond CK, Howaldstevenson I, Vater CA, Stevens TH. Morphological Classification of the Yeast Vacuolar Protein Sorting Mutants - Evidence for a Prevacuolar Compartment in Class-E Vps Mutants. Mol. Biol. Cell. 1992; 3:1389–1402. [PubMed: 1493335]
23. Rieder SE, Banta LM, Kohrer K, McCaffery JM, Emr SD. Multilamellar endosome-like compartment accumulates in the yeast vps28 vacuolar protein sorting mutant. Mol Biol Cell. 1996; 7:985–999. [PubMed: 8817003]
24. Doyotte A, Russell MRG, Hopkins CR, Woodman PG. Depletion of TSG101 forms a mammalian 'Class E' compartment: a multicisternal early endosome with multiple sorting defects. J. Cell Sci. 2005; 118:3003–3017. [PubMed: 16014378]
25. Nickerson DP, West M, Odorizzi G. Did2 coordinates Vps4-mediated dissociation of ESCRT-III from endosomes. J. Cell Biol. 2006; 175:715–720. [PubMed: 17130288]
26. Falguieres T, et al. In Vitro Budding of Intralumenal Vesicles into Late Endosomes Is Regulated by Alix and Tsg101. Mol. Biol. Cell. 2008; 19:4942–4955. [PubMed: 18768755]
27. Tran JH, Chen CJ, Emr S, Schekman R. Cargo sorting into multivesicular bodies in vitro. Proc. Natl. Acad. Sci. USA. 2009; 106:17395–17400. [PubMed: 19805166]
28. Shih SC, et al. Epsins and Vps27p/Hrs contain ubiquitin-binding domains that function in receptor endocytosis. Nat. Cell Biol. 2002; 4:389–393. [PubMed: 11988742]
29. Bilodeau PS, Urbanowski JL, Winistorfer SC, Piper RC. The Vps27p-Hse1p complex binds ubiquitin and mediates endosomal protein sorting. Nat. Cell Biol. 2002; 4:534–539. [PubMed: 12055639]
30. Raiborg C, et al. Hrs sorts ubiquitinated proteins into clathrin-coated microdomains of early endosomes. Nat. Cell Biol. 2002; 4:394–398. [PubMed: 11988743]
31. Mizuno E, Kawahata K, Kato M, Kitamura N, Komada M. STAM proteins bind ubiquitinated proteins on the early endosome via the VHS domain and ubiquitin-interacting motif. Mol. Biol. Cell. 2003; 14:3675–3689. [PubMed: 12972556]

32. Bache KG, Raiborg C, Mehlum A, Stenmark H. STAM and Hrs are subunits of a multivalent ubiquitin-binding complex on early endosomes. J. Biol. Chem. 2003; 278:12513–12521. [PubMed: 12551915]
33. Hicke L, Schubert HL, Hill CP. Ubiquitin-binding domains. Nat. Rev. Mol. Cell Biol. 2005; 6:610–621. [PubMed: 16064137]
34. Hurley JH, Lee S, Prag G. Ubiquitin binding domains. Biochem. J. 2006; 399:361–372. [PubMed: 17034365]
35. Raiborg C, Bache KG, Mehlum A, Stang E, Stenmark H. Hrs recruits clathrin to early endosomes. EMBO J. 2001; 20:5008–5021. [PubMed: 11532964]
36. Sachse M, Urbe S, Oorschot V, Strous GJ, Klumperman J. Bilayered clathrin coats on endosomal vacuoles are involved in protein sorting toward lysosomes. Mol. Biol. Cell. 2002; 13:1313–1328. [PubMed: 11950941]
37. Shields SB, et al. ESCRT ubiquitin binding domains function cooperatively during MVB cargo sorting. J. Cell Biol. 2009; 185:213–224. [PubMed: 19380877]
38. Alam SL, et al. Ubiquitin interactions of NZF zinc fingers. EMBO J. 2004; 23:1411–1421. [PubMed: 15029239]
39. Katzmann DJ, Stefan CJ, Babst M, Emr SD. Vps27 recruits ESCRT machinery to endosomes during MVB sorting. J. Cell Biol. 2003; 162:413–423. [PubMed: 12900393]
40. Bilodeau PS, Winistorfer SC, Kearney WR, Robertson AD, Piper RC. Vps27-Hse1 and ESCRT-I complexes cooperate to increase efficiency of sorting ubiquitinated proteins at the endosome. J. Cell Biol. 2003; 163:237–243. [PubMed: 14581452]
41. Saksena S, Wahlman J, Teis D, Johnson AE, Emr SD. Functional Reconstitution of ESCRT-III Assembly and Disassembly. Cell. 2009; 136:97–109. [PubMed: 19135892]
42. Im YJ, Wollert T, Boura E, Hurley JH. Structure and Function of the ESCRT-II-III Interface in Multivesicular Body Biogenesis. Dev. Cell. 2009; 17:234–243. [PubMed: 19686684]
43. Lenz M, Crow DJG, Joanny JF. Membrane Buckling Induced by Curved Filaments. Phys. Rev. Lett. 2009; 103
44. Gill DJ, et al. Structural insight into the ESCRT-I/-II link and its role in MVB trafficking. EMBO J. 2007; 26:600–612. [PubMed: 17215868]
45. Kostelansky MS, et al. Molecular architecture and functional model of the complete yeast ESCRT-I heterotetramer. Cell. 2007; 129:485–498. [PubMed: 17442384]
46. Teis D, Saksena S, Emr SD. Ordered Assembly of the ESCRT-III Complex on Endosomes Is Required to Sequester Cargo during MVB Formation. Dev. Cell. 2008; 15:578–589. [PubMed: 18854142]
47. Murk JLAN, et al. Endosomal compartmentalization in three dimensions: Implications for membrane fusion. Proc. Natl. Acad. Sci. USA. 2003; 100:13332–13337. [PubMed: 14597718]
48. Teo H, Perisic O, Gonzalez B, Williams RL. ESCRT-II, an endosome-associated complex required for protein sorting: Crystal structure and interactions with ESCRT-III and membranes. Dev. Cell. 2004; 7:559–569. [PubMed: 15469844]
49. Hierro A, et al. Structure of the ESCRT-II endosomal trafficking complex. Nature. 2004; 431:221–225. [PubMed: 15329733]
50. Lee HH, Elia N, Ghirlando R, Lippincott-Schwartz J, Hurley JH. Midbody targeting of the ESCRT machinery by a noncanonical coiled coil in CEP55. Science. 2008; 322:576–580. [PubMed: 18948538]
51. Angelova MI, Dimitrov DS. Liposome electroformation. Faraday Discuss. Chem. Soc. 1986; 81:303–311.

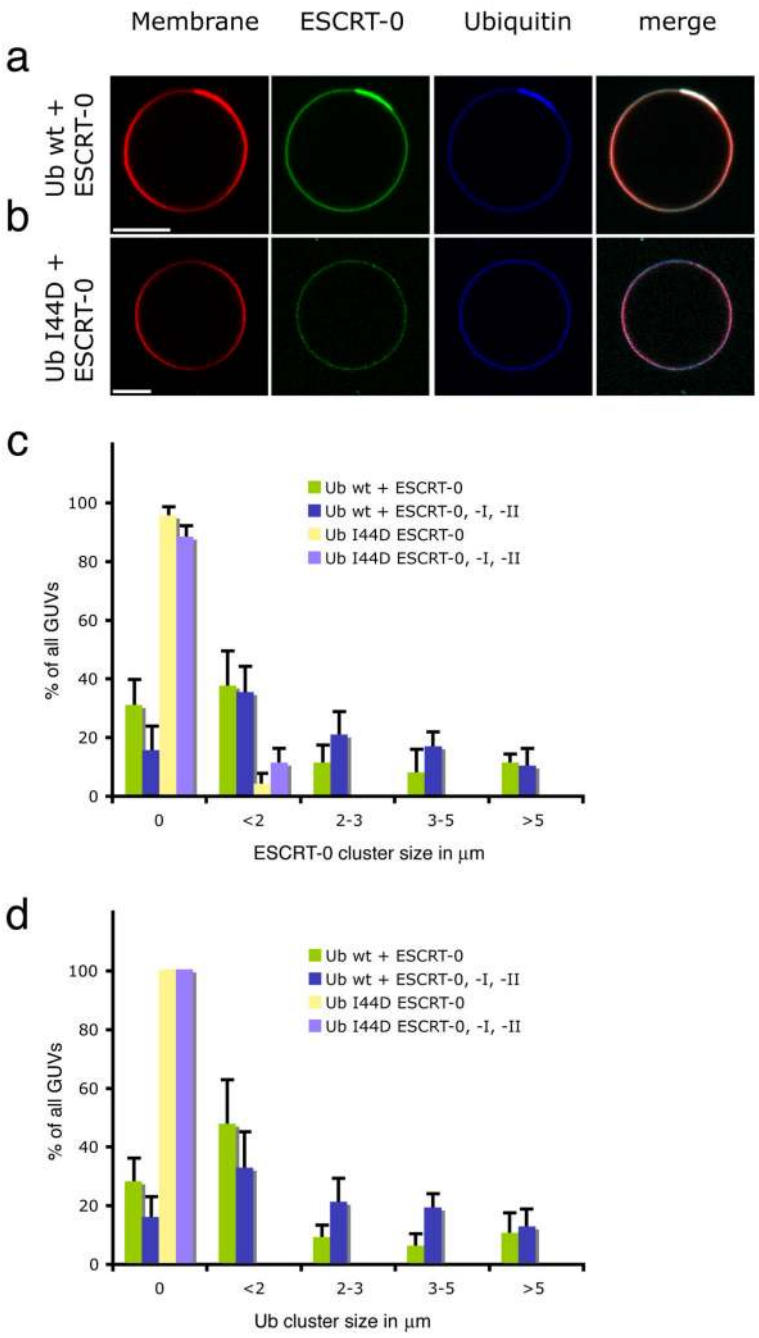

Fig. 1.

Model cargo clustering by ESCRT-0. **a**, ESCRT-0 induces the formation of Ub domains. (**b**) Ub mutant I44D is not clustered under the same conditions as in (**a**). Tagged Ub fusions were present at 65 nM. (**c**) Clusters of ESCRT-0 (15 nM, labeled with Alexa 488) can form in the presence of Ub I44D, but the size and number of clusters is reduced. The presence of 15 nM ESCRT-I and II has little effect on the clustering. (**d**) Ub-CFP clustering by ESCRT-0 is prevented in the I44D mutant. Error bars in (**c**) and (**d**) were calculated from the standard deviation of n = 3 separate experiments. Scale bar = 10 µm.

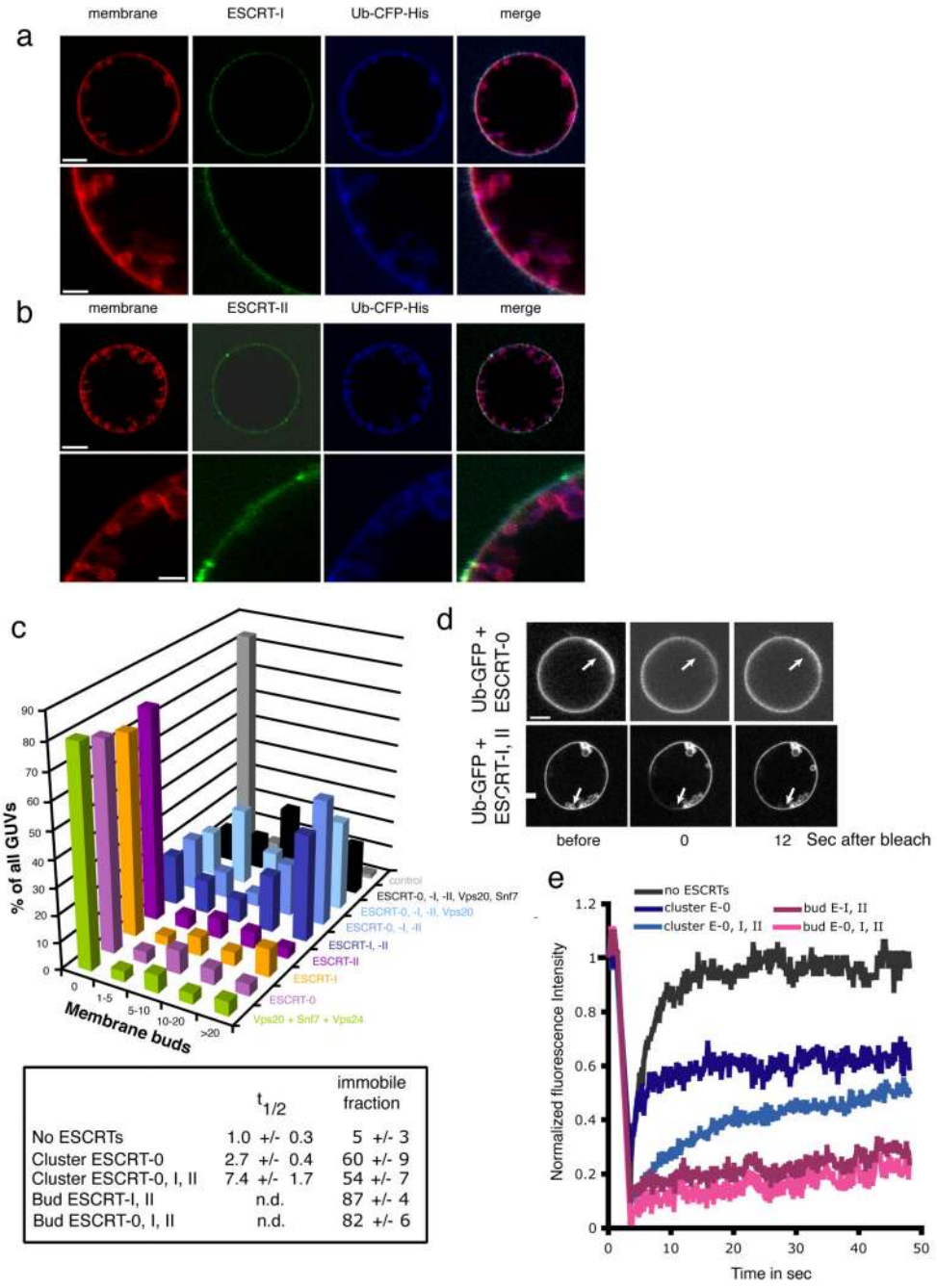

	$t_{1/2}$	immobile fraction
No ESCRTs	1.0 +/- 0.3	5 +/- 3
Cluster ESCRT-0	2.7 +/- 0.4	60 +/- 9
Cluster ESCRT-0, I, II	7.4 +/- 1.7	54 +/- 7
Bud ESCRT-I, II	n.d.	87 +/- 4
Bud ESCRT-0, I, II	n.d.	82 +/- 6

Fig. 2.

ESCRT-I and –II-induce membrane buds and confine cargo in them. Labeled ESCRT-I and unlabeled ESCRT-II (**a**) and vice versa (**b**) induce buds, as summarized (**c**). (**d, e**) Fluorescence recovery after photobleaching (FRAP) experiments of model cargo confined in buds. Arrows indicate buds in which Ub-GFP does not significantly recover on the time scale of the experiment. Error bars in were calculated from the standard deviation of n = 3 separate experiments in part (**c**) and for n = 10 different buds each selected from a different GUV in (**e**). Scale bar = 10 μm.

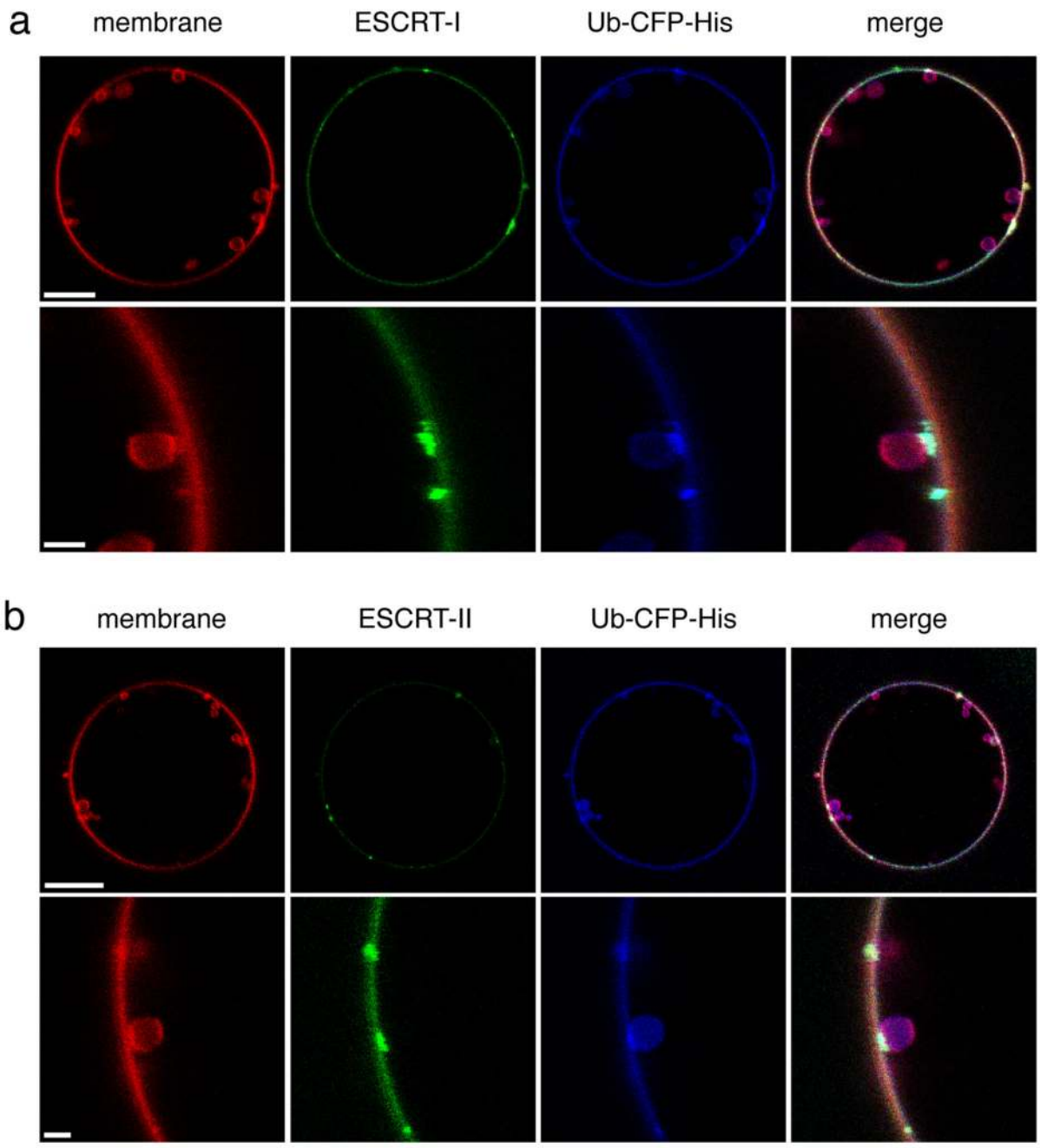

Fig. 3.

ESCRT-I and II localize to the necks of membrane buds. Imaging was carried out in the presence of 15 nM unlabeled Vps20, which binds to ESCRT-II and augments ESCRT-I and II occupancy at the neck. ESCRT-I and –II were present at 15 nM each in both experiments. Labeled ESCRT-I in the presence of unlabeled ESCRT-II (**a**) and labeled ESCRT-II in the presence of unlabeled ESCRT-I (**b**) induce membrane buds and co-localize with their necks. Scale bar = 10 μm and 2 μm (insets).

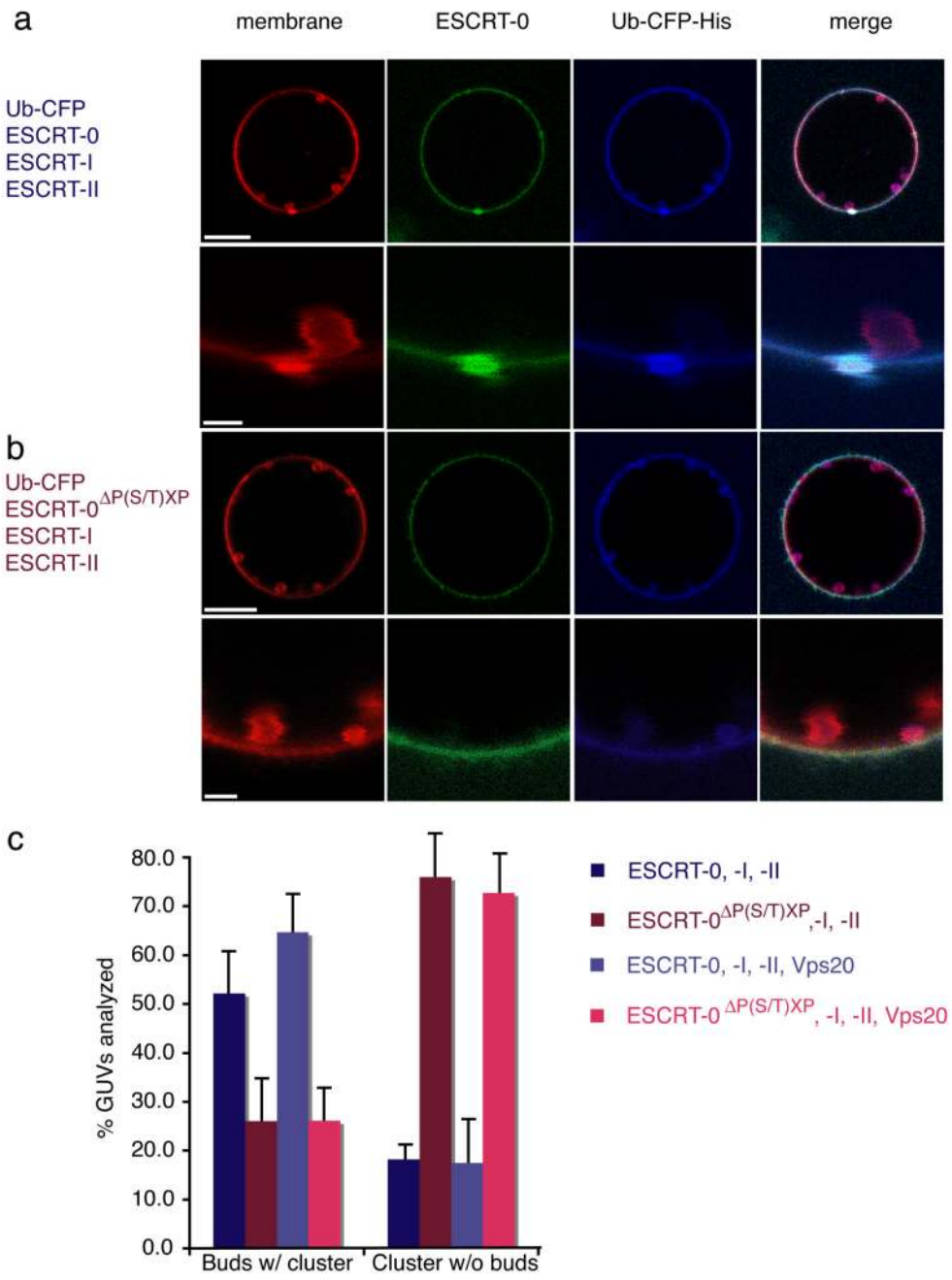

Fig. 4.

ESCRT-0 Ub domains co-localize with ESCRT-I-II membrane buds. (**a**) Wildtype yeast ESCRT-0 (15 nM, Alexa 488-labelled) in the presence of 65 nM His_6-Ub-CFP colocalizes with buds induced by 15 nM each unlabelled ESCRT-I and –II. The second row shows a close-up of an individual cluster-bud pair. (**b**) ESCRT-0 mutated in three P(S/T)XP motifs required for ESCRT-I binding does not colocalizes with membrane buds. (**c**) Results for 70 GUVs are summarized in histograms. Error bars in were calculated from the standard

deviation of n = 3 separate experiments. Scale bar = 10 μm (upper panels showing entire GUV) and 2 μm (inset).

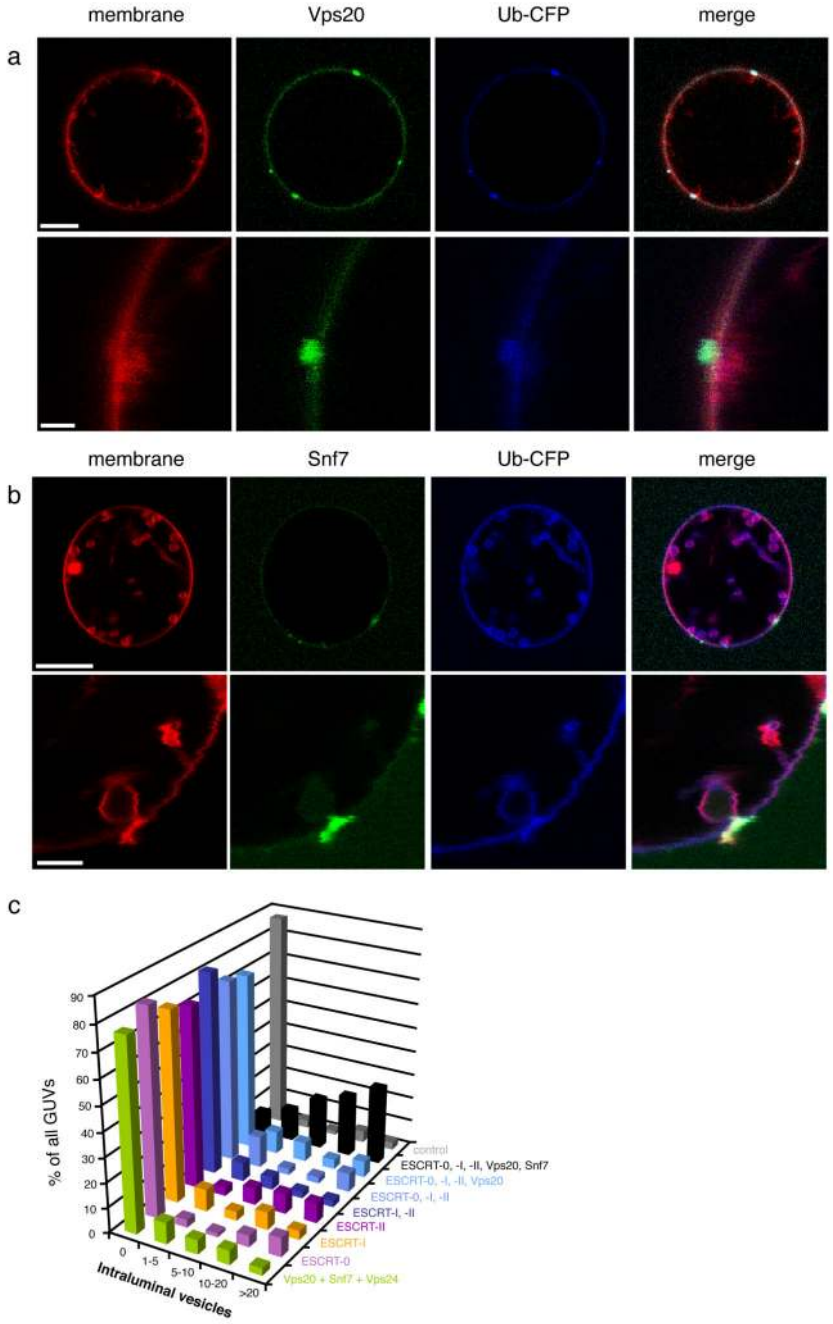

Fig. 5.

ESCRT-III localizes to bud necks for membrane scission. 15 nM each of unlabeled ESCRT-0, ESCRT-I, and ESCRT-II, and 65 nM of His-Ub-GFP were present in both experiments. **a**,Vps20 (15 nM, labeled with Alexa 488) is localized to bud necks but does not sever the necks. **b**, Snf7 (15 nM, labeled with Alexa 488) localizes to bud necks when Vps20 (15 nM, unlabeled) is present. (**c**) The dependence of ILV production on Snf7 is indicated by the histogram of observations on 100 GUVs. Error bars in were calculated from

the standard deviation of n = 3 separate experiments. Scale bar = 10 μm (upper panels showing entire GUV) and 2 μm (inset).

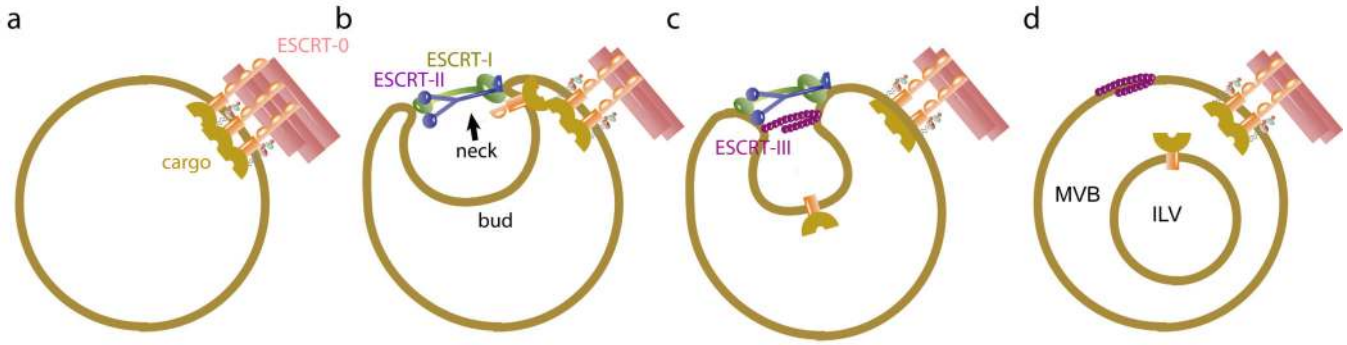

Fig. 6.

Molecular mechanism of MVB biogenesis. **a**, ESCRT-0 self-assembles and clusters cargo. **b**, The ESCRT-I and –II contain multiple membrane binding sites separated by a rigid stalk in ESCRT-I and a rigid Y-structure in ESCRT-II that could prop open membrane necks. **c**, ESCRT-II recruits Vps20 to the neck, which in turn recruits Snf7, the main engine for neck scission. **d**, Following scission, cargo is internalized in ILVs while ESCRT-III remains on the outside of the limiting membrane until it is recycled by Vps4.